AIP Applied Physics Letters

Role of nucleation sites on the formation of nanoporous Ge

B. R. Yates, B. L. Darby, R. G. Elliman, and K. S. Jones

Citation: Appl. Phys. Lett. **101**, 131907 (2012); doi: 10.1063/1.4755886
View online: http://dx.doi.org/10.1063/1.4755886
View Table of Contents: http://apl.aip.org/resource/1/APPLAB/v101/i13
Published by the American Institute of Physics.

Related Articles

Analysis of optical properties of porous silicon nanostructure single and gradient-porosity layers for optical applications
J. Appl. Phys. 112, 053506 (2012)

Holographic modification of TiO2 nanostructure for enhanced charge transport in dye-sensitized solar cell
J. Appl. Phys. 112, 043110 (2012)

Universal ultrafast sandpaper assisting rubbing method for room temperature fabrication of two-dimensional nanosheets directly on flexible polymer substrate
Appl. Phys. Lett. 101, 073113 (2012)

Local structure, paramagnetic properties, and porosity of natural coals: Spectroscopic studies
J. Appl. Phys. 112, 043504 (2012)

Surface-plasmon-like modes of graphite powder compact in microwave heating
J. Appl. Phys. 112, 034905 (2012)

Additional information on Appl. Phys. Lett.

Journal Homepage: http://apl.aip.org/
Journal Information: http://apl.aip.org/about/about_the_journal
Top downloads: http://apl.aip.org/features/most_downloaded
Information for Authors: http://apl.aip.org/authors

ADVERTISEMENT

Role of nucleation sites on the formation of nanoporous Ge

B. R. Yates,[1,a)] B. L. Darby,[1] R. G. Elliman,[2] and K. S. Jones[1]
[1]*Department of Materials Science and Engineering, University of Florida, Gainesville, Florida 32611-6400, USA*
[2]*Department of Electronic Materials Engineering, Research School of Physical Sciences and Engineering, Australian National University, Canberra, Australian Capital Territory 0200, Australia*

(Received 15 August 2012; accepted 14 September 2012; published online 26 September 2012)

The role of nucleation sites on the formation of nanoporous Ge was investigated. Three Ge films with different spherical or columnar pore morphologies to act as inherent nucleation sites were sputtered on (001) Ge. Samples were implanted 90° from incidence at 300 keV with fluences ranging from 3.0×10^{15} to 3.0×10^{16} Ge^+/cm^2. Electron microscopy investigations revealed varying thresholds for nanoporous Ge formation and exhibited a stark difference in the evolution of the Ge layers based on the microstructure of the initial film. The results suggest that the presence of inherent nucleation sites significantly alters the onset and evolution of nanoporous Ge. © *2012 American Institute of Physics*. [http://dx.doi.org/10.1063/1.4755886]

The decomposition of crystalline Ge (c-Ge) into a nanoporous network following heavy ion irradiation has been studied for several decades.[1–10] The nanoporous structure, widely believed to form due to a barrier to point defect recombination resulting in vacancy clustering and subsequent pore growth during implantation,[1–3] is characterized by a fibrous or sponge-like network of amorphous Ge. Recently, there is renewed interest in this topic with attention focusing on deposited Ge films. Romano *et al.* and Impellizzeri *et al.* have investigated the formation of the nanoporous structure in deposited Ge films following self-implantation and have found that the structure is significantly different from that formed in crystalline Ge (c-Ge), an effect which was attributed to the voids in the initial film.[11–13] In addition, there has been interest in the specific application of nanoporous Ge, where it has been used as a high-performance anode for lithium ion battery applications.[14]

In this work, a systematic study of pre-existing voids on the formation of nanoporous Ge during ion-irradiation is conducted. The influence of a vertical interface on the structural evolution of nanoporous Ge is also investigated in this study.

A heterostructure consisting of alternating 300 nm Ge and 25 nm Si films was sputter deposited onto (001) Ge (c-Ge). The Ge layers were deposited at a rate of 6.4 nm min^{-1} using different substrate temperatures and Ar sputtering gas pressures to alter their microstructure. The first Ge layer (Ge_C) was deposited with the substrate held at 450 °C and an Ar pressure of 5 mT, the second layer (Ge_B) was deposited with the substrate at 20 °C and an Ar pressure of 1 mT, and the third layer (Ge_A) was deposited with the substrate at 20 °C and an Ar pressure of 3 mT. The Si layers were deposited primarily to separate neighboring Ge layers and were deposited with the substrate of 20 °C and an Ar pressure of 5 mT. Following the depositions, the substrate was diced into sections and then glued "face to face" with M-Bond 610 such that the deposited films were in close proximity. In Fig. 1(a), a schematic diagram of the as-deposited heterostructure on (001) c-Ge is shown as deposited (left) and as rotated and glued (right). The (011) faces (perpendicular to the glue line) of the c-Ge were mechanically polished to a mirror finish by using a MultiPrep polishing system. Polished sections were then Ge^+ implanted normal to the polished surface with 300 keV to fluences ranging from 3.0×10^{15} to 3.0×10^{16} Ge^+/cm^2. Plan-view scanning electron microscopy (SEM) was used to characterize the implanted structures. Cross-sectional transmission electron microscopy (TEM) investigations were completed using a JEOL 2010 F with samples prepared through focused ion beam (FIB) milling using an FEI DB235. The as-sputtered layers on Ge were characterized using energy-dispersive x-ray spectroscopy (EDS) in the TEM using scanning TEM (STEM) mode to estimate the density of the films as described below.

Fig. 1(b) shows a cross-sectional TEM (XTEM) image of the rotated and glued Ge/Si heterostructure. The subtle changes in deposition conditions yielded significant differences in the microstructures of the deposited films. Ge_C yielded a columnar structure with 3–5 nm wide columnar pores in the direction of film growth similar to that reported by Romano *et al.*[12] In contrast, Ge_B consisted of a matrix of small voids with a diameter on the order of 2.5–4 nm and Ge_A contained larger voids approximately 5–6.5 nm in diameter. All Ge layers were amorphous as confirmed by electron diffraction.

The film densities were estimated by acquiring an EDS line scan parallel to the sample surface. In doing so, it was assumed that the sample thickness was constant across the investigated length; therefore, a modification of the Castaing approximation[15] becomes

$$\rho_{spt-Ge} = \left(\frac{I_{spt-Ge}}{I_{c-Ge}}\right) \times \rho_{c-Ge}, \quad (1)$$

where $I_{spt\text{-}Ge}$ and $\rho_{spt\text{-}Ge}$ are the average x-ray counts and density of the sputtered film and $I_{c\text{-}Ge}$ and $\rho_{c\text{-}Ge}$ are the average x-ray counts and density of c-Ge, a known value of

a)Author to whom correspondence should be addressed. Electronic mail: bradyates@ufl.edu.

 © 2012 American Institute of Physics

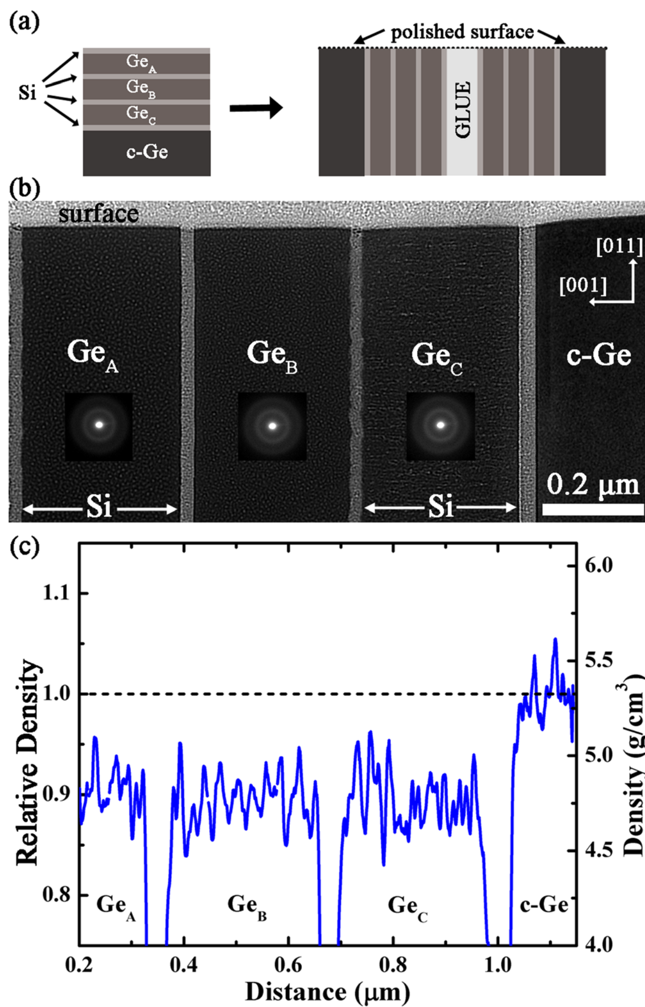

FIG. 1. (a) Schematic of Ge/Si heterostructure after deposition (left) and subsequent gluing of samples (right). (b) XTEM image of the initial Ge/Si heterostructure consisting of 5–6.5 nm pores (Ge_A), 2.5–4 nm spherical pores (Ge_B), and 3–5 nm wide columnar pores (Ge_C) separated by 25 nm layers of Si as-grown on (001) Ge (c-Ge). Inset selected area diffraction patterns display the amorphous nature of the as-deposited films. (c) EDS line scan intensity as a function of distance across the heterostructure normalized to the known density of the c-Ge substrate.

$5.32\ \mathrm{g\ cm^{-3}}$.[16] Using this equation, the ratio of average x-ray intensity of a sputtered film with the c-Ge substrate from an EDS line scan can be used to determine the density of each individual film where a measured deviation in intensity can be directly correlated to a change in film density. A similar method using relative x-ray intensities to calculate an unknown weight percentage has also been documented.[17,18]

Fig. 1(c) shows the normalized densities for the sputtered layers as determined using the Castaing approximation. The three sputtered films have a measured average density of $4.87 \pm 0.40\ \mathrm{g\ cm^{-3}}$, $4.76 \pm 0.35\ \mathrm{g\ cm^{-3}}$, and $4.77 \pm 0.35\ \mathrm{g\ cm^{-3}}$ for Ge_A, Ge_B, and Ge_C, respectively. Despite the different microstructures, the macroscopic density of the sputtered films is approximately equal suggesting that either the pore volume is similar in each case or that it has a small effect on the macroscopic density.[12] The estimated density values are in reasonable agreement with previous reports of sputtered Ge densities.[19–21]

Fig. 2 shows the microstructural evolution of the deposited Ge layers after implanting Ge^+ to fluences of 3.0×10^{15},

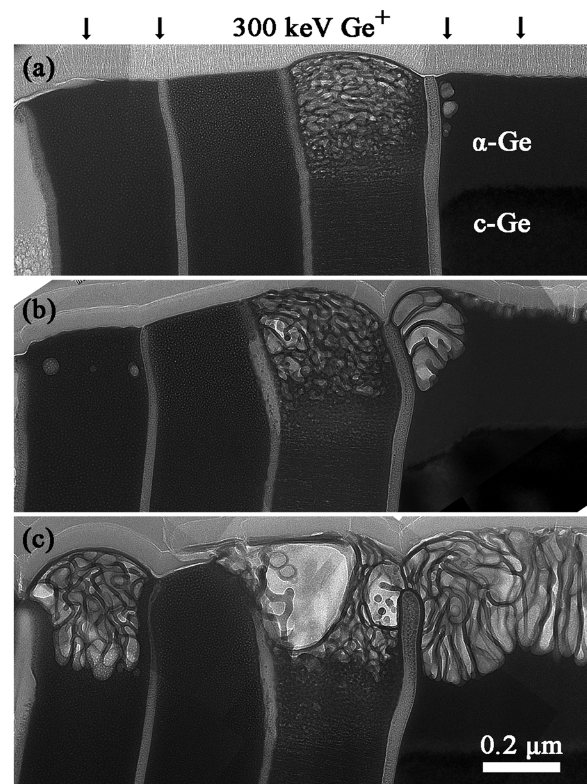

FIG. 2. Cross-sectional micrographs displaying the microstructural evolution of the Ge/Si heterostructure following implantation at 300 keV to a fluence of (a) $3.0 \times 10^{15}\ Ge^+/cm^2$, (b) $1.0 \times 10^{16}\ Ge^+/cm^2$, and (c) $3.0 \times 10^{16}\ Ge^+/cm^2$.

7.5×10^{15}, and $3.0 \times 10^{16}\ Ge^+/cm^2$ at 300 keV. Across the investigated fluence regime, in contrast to the columnar or fibrous structures formed in c-Ge, the deposited films decomposed into a network of spherical pores and also decomposed uniquely based on the initial microstructure of the film. Following a fluence of $3.0 \times 10^{15}\ Ge^+/cm^2$, Ge_C was nearly fully nanoporous to a depth of 350 nm with small pores elongated in the growth direction similar to the voids evident in the initial microstructure. However, Ge_A and Ge_B behave quite differently in that neither layer displayed any indication of nanoporous Ge formation. It should be noted that this Ge^+ fluence and energy has been reported to be above the threshold for nanoporous Ge formation in sputtered Ge films.[12]

As the fluence was increased to $1.0 \times 10^{16}\ Ge^+/cm^2$, nanoporous Ge_C further decomposed to form larger pores; however, the depth of the nanoporous layer did not change, remaining at approximately 350 nm. In Ge_A, the formation of singular spherical pores was evident across the width of the layer. The pores were spherical in nature and were approximately 10–50 nm in diameter at a depth of approximately 90 nm from the surface.

Following implantation to a fluence of $3.0 \times 10^{16}\ Ge^+/cm^2$, Ge_A, Ge_C, and c-Ge fully decomposed into nanoporous Ge to a similar depth of approximately 350 nm. Ge_A formed a sponge-like nanoporous microstructure in contrast to the horizontally elongated pores observed in Ge_C. Large bubble-like structures were evident in Ge_C, which is believed to be due to early onset of decomposition in this layer and subsequent evolution into this morphology. However, Ge_B has not formed the characteristic nanoporous structure. High-

resolution TEM images of Ge_B (not shown) of the implanted depth have shown that pre-existing pores have coalesced to form larger pores, which give credence to the notion that Ge_B is approaching the threshold fluence for decomposition into nanoporous Ge.

Fig. 3 displays the microstructural evolution of the Ge_C/c-Ge interface as a function of fluence from 3.0×10^{15} to 1.0×10^{16} Ge^+/cm^2. In Fig. 3(a), it is evident that pores form in close proximity to the Ge_C/c-Ge interface with the pore distribution centered at approximately 75 nm from the surface similar to what is observed in the Ge_A layer in Fig. 2(b). This depth corresponds well with the projected range of the damage (R_D) as simulated by the stopping range of ions in matter (SRIM) and is overlaid on the image for comparison.[22] Increasing fluence further increases the size and number of pores observed at the interface as well as localized swelling. After implanting to a fluence of 1.0×10^{16} Ge^+/cm^2, the near-interface volume is decomposed into the characteristic nanoporous structure to a depth of 250 nm; however, it is also obvious that the pores propagate perpendicular to the direction of the beam rather than the characteristic vertical direction observed in bulk c-Ge. The direction of propagation is presently believed to be solely due to the nature and location of the pore nuclei and not the direction of the ion beam. For both bulk c-Ge and near-interface c-Ge, the pores propagate away from the pore nuclei. The horizontal pore propagation of near-interface Ge is to be due to the nucleation of pores occurring at the Ge/Si interface and not at the surface as is the case for bulk c-Ge.

Fig. 2(c) exhibits further contrasts between the decomposition of near-interface and bulk c-Ge. The morphological difference between the nanoporous structure of c-Ge near the Ge_C/c-Ge as compared to bulk c-Ge is evident where the near-interface c-Ge pores exhibit a swirling morphology, while the pores in the bulk c-Ge are vertical as has been observed previously.[1–4] The increased swelling of the near-interface Ge as compared to bulk c-Ge (see Fig. 2(b)) also raises questions regarding the theory that swelling is proportional to the deposited nuclear energy[12,23] as this should be assumed to be constant regardless of interface proximity.

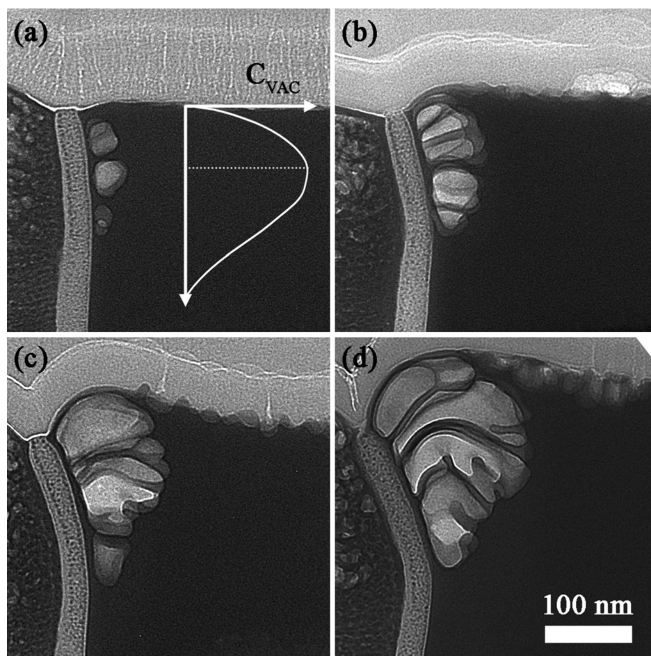

FIG. 3. Cross-sectional micrographs of the Ge_C/c-Ge interface (near-interface c-Ge) following implantation at 300 keV to a fluence of (a) 3.0×10^{15} Ge^+/cm^2, (b) 5×10^{15} Ge^+/cm^2, (c) 1.0×10^{16} Ge^+/cm^2, and (d) 1.0×10^{16} Ge^+/cm^2. Vacancy profile as simulated by SRIM is overlaid in (a).

Fig. 4 displays images of the Ge_C/c-Ge interface following implantation to a fluence of 1.0×10^{16} Ge^+/cm^2 as characterized by SEM (a) and XTEM (b) displaying the varying contrast between nanoporous films and c-Ge. Romano *et al.* observed this contrast difference in sputtered nanoporous films and attributed it to the depth and size of pores being different from that of c-Ge.[12] Impellizzeri *et al.* also observed a reduction in contrast for molecular beam epitaxially deposited films and attributed it to the different resulting pore morphologies.[13] However, the images in Fig. 4 show that it is not an issue of pore morphology, but rather the presence of a thin 5-10 nm layer on the surface of deposited films as well as the near-interface c-Ge that is reducing imaging contrast. The surface covering of the near-interface c-Ge extends approximately 150 nm away from the Si interface and is also observed in Figs. 2(c) and 3. The surface covering was analyzed using EDS (not shown) and was determined to be composed of Ge. Fig. 4 also demonstrates the horizontal nature of the pore walls as they extend laterally from the interface into the bulk c-Ge.

For c-Ge, it has been widely believed that pores nucleate at the Ge surface and propagate into the bulk upon further irradiation.[1–4,23,24] However, this work has shown that the formation of nanoporous Ge is highly dependent on the presence of nucleation sites. For sputtered Ge films, the nucleation sites can be assumed to be pre-existing pores in the film that acts as vacancy sinks, which allows for pore expansion and growth during implantation. Previously, it has been suggested that sub-surface voids are the precursor to nanoporous Ge formation.[25,26] However, sub-surface voids were not observed for bulk c-Ge and thus it is presently proposed that surface roughening is the precursor to nanoporous Ge formation in bulk c-Ge (see Fig. 3). It is suggested that bulk c-Ge does not rely on inherent nucleation sites, but rather surface roughness for the formation of nanoporous Ge.

The presence of pores in the near-interface region that occurs at a fluence nearly an order of magnitude lower than the formation of the nanoporous structure in bulk c-Ge is

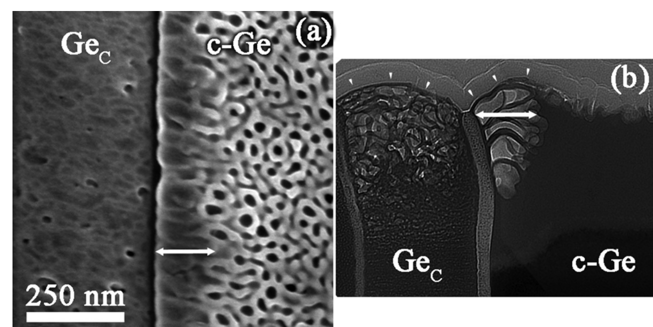

FIG. 4. (a) Plan-view SEM and (b) XTEM micrographs of the Ge_C/c-Ge interface displaying the thin surface covering evident in the deposited layers as well as in the near-interface c-Ge following implantation at 300 keV to a fluence of 1.0×10^{16} Ge^+/cm^2. The double white arrows indicate the approximate width of the surface covering in the c-Ge substrate.

certainly interesting. For near-interface c-Ge, it is suggested that the interface provides an interstitial sink[27,28] thereby allowing an excess vacancy population, which similar to pre-existing pores in deposited films, enables the decomposition into porous Ge at the implant R_D with a reduced fluence threshold. Further evidence of this is found in that spherical voids near the R_D were observed in Ge_A following a 1.0×10^{16} Ge^{+}/cm^2 implant. Pore nucleation at inherent sites is characterized as having a thin surface layer that is observed for all deposited films as well as for near-interface c-Ge. The pores centered around the R_D strongly suggest the presence of pre-existing nucleation sites that spur pore formation and gives further evidence that a vacancy clustering mechanism is responsible for the formation of nanoporous Ge. In conjunction with these present findings, previous reports have shown that a buried nanoporous Ge layer is possible due to chemical nucleation sites where high concentrations of implanted iodine act as a nucleation site.[8,23]

The formation of nanoporous Ge is highly dependent on the nucleation sites present in the films prior to implantation. In contrast to the open pore structure that is observed in bulk nanoporous c-Ge due to surface roughness, it has been shown that inherent nucleation sites allow the formation of pores at the implant R_D at a reduced implant threshold. When this occurs, it is characterized by a thin surface covering in both deposited films and near-interface c-Ge. The results show that careful engineering of the initial Ge microstructure can allow for radically different microstructures and can reduce the critical fluence threshold required for nanoporous Ge formation for future applications.

The authors acknowledge the Intel Corporation for funding this work, the Major Analytical Instrumentation Center and the Nanoscale Research Facility at the University of Florida for access to their facilities, and support from the Australian Government's NCRIS/EIF programs for access to Heavy Ion Accelerator Facilities at the Australian National University. The authors also acknowledge Y. Yang (University of Florida) for the use of the MultiPrep equipment.

[1] I. H. Wilson, J. Appl. Phys. **53**, 1698 (1982).
[2] B. R. Appleton, Appl. Phys. Lett. **41**, 711 (1982).
[3] O. W. Holland, B. R. Appleton, and J. Narayan, J. Appl. Phys. **54**, 2295 (1983).
[4] B. R. Appleton, O. W. Holland, D. B. Poker, J. Narayan, and D. Fathy, Nucl. Instrum. Methods Phys. Res. B **7–8** (Pt 2), 639 (1985).
[5] L. M. Wang and R. C. Birtcher, Appl. Phys. Lett. **55**, 2494 (1989).
[6] L. M. Wang and R. C. Birtcher, Philos. Mag. A **64**, 1209 (1991).
[7] R. C. Birtcher, Philos. Mag. B **73**, 677 (1996).
[8] H. Huber, W. Assmann, S. A. Karamian, A. Mücklich, W. Prusseit, E. Gazis, R. Grötzschel, M. Kokkoris, E. Kossionidis, H. D. Mieskes, and R. Vlastou, Nucl. Instrum. Methods Phys. Res. B **122**, 542 (1997).
[9] B. Stritzker, R. Elliman, and J. Zou, Nucl. Instrum. Methods Phys. Res. B **175–177**, 193 (2001).
[10] S. G. Mayr and R. S. Averback, Phys. Rev. B **71**, 134102 (2005).
[11] L. Romano, G. Impellizzeri, M. V. Tomasello, F. Giannazzo, C. Spinella, and M. G. Grimaldi, J. Appl. Phys. **107**, 084314 (2010).
[12] L. Romano, G. Impellizzeri, L. Bosco, F. Ruffino, M. Miritello, and M. G. Grimaldi, J. Appl. Phys. **111**, 113515 (2012).
[13] G. Impellizzeri, L. Romano, L. Bosco, C. Spinella, and M. G. Grimaldi, Appl. Phys. Express **5**, 035201 (2012).
[14] N. G. Rudawski, B. L. Darby, B. R. Yates, K. S. Jones, R. G. Elliman, and A. A. Volinsky, Appl. Phys. Lett. **100**, 083111 (2012).
[15] R. Castaing, Ph.D. dissertation, University of Paris, 1951.
[16] *Springer Handbook of Condensed Matter and Materials Data*, edited by W. Martienssen and H. Warlimont (Springer, Heidelberg/New York, 2005).
[17] L. S. Birks, J. Appl. Phys. **31**, 1297 (1960).
[18] L. S. Birks, J. Appl. Phys. **32**, 387 (1961).
[19] S. Koc, O. Renner, M. Závětová, and J. Zemek, Czech. J. Phys. **22**, 1296 (1972).
[20] T. M. Donovan, E. J. Ashley, and W. E. Spicer, Phys. Lett. A **32**, 85 (1970).
[21] T. M. Donovan, W. E. Spicer, and J. M. Bennett, Phys. Rev. Lett. **22**, 1058 (1969).
[22] J. F. Ziegler, Nucl. Instrum. Methods Phys. Res. B **219–220**, 1027 (2004).
[23] T. Steinbach, J. Wernecke, P. Kluth, M. C. Ridgway, and W. Wesch, Phys. Rev. B **84**, 104108 (2011).
[24] T. Janssens, C. Huyghebaert, D. Vanhaeren, G. Winderickx, A. Satta, M. Meuris, and W. Vandervorst, J. Vac. Sci. Technol. B **24**, 510 (2006).
[25] N. Nitta, M. Taniwaki, Y. Hayashi, and T. Yoshiie, J. Appl. Phys. **92**, 1799 (2002).
[26] B. L. Darby, B. R. Yates, N. G. Rudawski, K. S. Jones, A. Kontos, and R. G. Elliman, Thin Solid Films **519**, 5962 (2011).
[27] R. Raman, M. E. Law, V. Krishnamoorthy, K. S. Jones, and S. B. Herner, Appl. Phys. Lett. **74**, 1591 (1999).
[28] V. Krishnamoorthy, M. Puga Lambers, and K. S. Jones, Defect Diffus. Forum **183–185**, 189 (2000).